Oxygen impurity effects at metal/silicide interfaces: Formation of silicon oxide and suboxides in the Ni/Si system[a)]

P. J. Grunthaner and F. J. Grunthaner

Jet Propulsion Laboratory, California Institute of Technology, Pasadena, California 91109

D. M. Scott and M-A. Nicolet

California Institute of Technology, Pasadena, California 91125

J. W. Mayer

Cornell University, Ithaca, New York 14853

(Received 20 March 1981; accepted 23 June 1981)

The effect of oxygen impurities on the Ni/Ni_2Si interface has been investigated via ion implantation using x-ray photoelectron spectroscopy (XPS), $^4He^+$ backscattering, and $^{16}O(d,\alpha)^{14}N$ nuclear reactions. Oxygen dosages corresponding to peak concentrations of 1, 2, and 3 atomic percent were implanted into Ni films evaporated on Si (100) substrates. The oxygen, nickel, and silicon core lines were monitored as a function of time during *in situ* growth of the Ni silicide to determine the chemical nature of the diffusion barrier known to form in the presence of oxygen impurities. It is shown that neither Ni oxide or mixed compounds such as Ni_2SiO_4 are involved in the barrier formation. The data demonstrate that as the advancing Ni/Ni_2Si interface encounters oxygen in the Ni film, silicon suboxides (Si_2O_3, Si_2O, and SiO) are formed. As more oxygen is encountered, Si takes on a full coordination of oxygen, forming SiO_2. When a sufficient layer of SiO_2 has formed, Ni metal is no longer able to diffuse through to the Si/Ni_2Si interface to continue the solid phase reaction. It has been determined under UHV annealing conditions that the amount of oxygen necessary to stop the Ni diffusion is 2.2×10^{16} O/cm^2. These experiments also provide a novel approach for synthesizing Si oxides and suboxides in a metallic matrix for examining relaxation effects in XPS as well as providing model compounds for Si/SiO_2 interfacial studies.

PACS numbers: 73.40.Sx, 61.70.Wp

I. INTRODUCTION

The relative importance of interfaces and interfacial reactions in microelectronic processing technology has stimulated a significant research effort on the careful study of surface reactions on clean and well-characterized substrates. Too often, interface models of thin-film reactions are idealized without consideration of the role played by the unavoidable presence of impurities. Such impurities can modify the defect distribution, change the surface free energy, decorate grain boundaries, and form reaction barriers. These contributions can change the reaction kinetics and may indeed modify the identity of the final reaction product. In this work, we examine the effect of oxygen impurities on the Ni/Ni_2Si interface using ion-implantation techniques as a controlled source of oxygen, and x-ray photoemission, Rutherford backscattering spectroscopy, and $^{16}O(d,\alpha)^{14}N$ nuclear reactions as the methods of structural characterization. The accumulation of oxygen at the interface in these silicide reactions and the subsequent formation of a reaction barrier have been reported previously by other workers.[1-3] In this effort, we concentrate on the chemical nature of this diffusion barrier.

These experiments result in the preparation of thin oxide films (5–25 Å) sandwiched between a thin Ni^0 layer and an extended Ni_2Si substrate. The Ni_2Si silicide is a semimetal and, consequently, these thin silicon oxides are layered between two metallic structures. This metal/oxide/metal system provides a straightforward synthetic method for the preparation of $SiO_2(Si^{+4})$, $Si_2O_3(Si^{+3})$, $SiO(Si^{+2})$, and $Si_2O(Si^{+1})$ species. In our previous work,[4-7] we have demonstrated the presence of the intermediate oxidation states of silicon at the Si/SiO_2 interface, synthesized these species as bulk powders, studied their oxidative interconversion, and suggested their presence in the radiation-induced damage mechanism in thermal SiO_2. This analysis has been based on the study of binding energy shifts of core levels as determined by high-resolution x-ray photoemission. In the course of this work, we have suggested that the Si-to-O charge transfer entailed in the Si–O bond is strongly modulated by variations in the Si–O–Si bridging bond angle.[4] This concept of structure-induced charge transfer (SICT) would require that as the Si–O–Si bond responds to strain introduced by lattice mismatch, an appropriate chemical shift can be observed in the XPS spectrum.

The observed shifts in XPS core level binding energies can be represented as the sum of the true chemical shift and the

 0022-5355/81/030641-08$01.00

change in final-state relaxation energy

$$\Delta E_{BE} = \Delta E_{\text{chem}} + \Delta E_{\text{relax}}. \quad (1)$$

Our previous analysis of chemical shifts in the Si–O system is based on the assumption that the change in relaxation energy between Si^0 and SiO_2 is proportional to the change in charge transfer. In this metal/oxide/metal system, however, the relaxation term of Eq. (1) is dominated by the presence of the metallic overlayer and substrate. Therefore, the observed changes in relative binding energy should be a measure of the actual chemical shift for these SiO_x species. Finally, the preparation of SiO_2 films grown on different substrates and with differing metal overlayers makes it possible to observe $SiO_{4/2}$ tetrahedra in different strain environments. In the following, we examine the binding energies as obtained and relate them to the SICT model. Throughout these discussions, we emphasize the use of binding-energy differences to establish the direction and extent of change transfer. These binding-energy differences are taken between core levels corresponding to the atoms participating in a particular bond.

II. EXPERIMENTAL

The results reported here were obtained using commercial n-type (100) Si substrates with a resistivity of 1–10 Ω cm. The Si wafers were cleaned ultrasonically with trichloroethylene (TCE), acetone, and methanol and then rinsed with deionized water. Just prior to loading for evaporation, the substrate was etched in dilute HF and rinsed again in deionized water. Nickel films, 1280 Å in thickness, were e-beam evaporated at ~35 Å/s with a background pressure of $\sim 5 \times 10^{-7}$ Torr.

Several wafers were then implanted with 7.64×10^{15} cm^{-2}, 1.54×10^{16} cm^{-2} and 2.34×10^{16} cm^{-2} of $^{16}O^+$ at 80 KeV. This corresponds to a gaussian oxygen distribution centered ~640 Å below the Ni surface with peak concentrations of 1, 2, and 3 at.%, respectively. The standard deviation, σ, of the oxygen distribution is ~330 Å. The background pressure during implantation was $\sim 5 \times 10^{-7}$ Torr.

These sample preparations resulted in the presence of a significant carbon overlayer on the Ni surfaces which could not be removed with a variety of solvents (ethanol, TCE, acetone, methyl ethyl ketone) or acid etches (HCl, HF). We attribute this carbon overlayer to a pump oil contamination obtained during the ion implantation step which had been subsequently polymerized by the implantation process. The carbon contamination could only be removed by plasma oxidation. The samples were placed in a flowing N_2 dry box and first rinsed with ethanol. They were then oxidized for 10 min in an O_2 plasma at a pressure of ~50 mTorr. The nickel oxide that had formed during the oxidation was etched off by spinning the sample at 3600 rpm and adding dropwise 500 μl of 1:1 HCl in ethanol followed by 1000 μl of ethanol. The sample inlet port of the spectrometer is connected directly to the N_2 dry box. Consequently, no further oxygen or carbon contamination occurred after etching.

After establishing sample surfaces that are free of oxide and carbon overlayer contamination, the Ni 2p, Si 2p, and O 1s core levels were monitored as the samples were heated *in situ* to 550 K in the analyzer chamber of the XPS spectrometer. This spectrometer is a modified HP5950A system (1486.6 eV photon energy). Only one core level was monitored as a function of time per sample. The vacuum inside the chamber during heating was better than 2×10^{-9} Torr. After the samples had reacted completely, they were cooled to 298 K to allow for extended data accumulation on the final product.

After XPS analysis, the final oxygen distribution for each of the three implant dosages was measured by the $^{16}O(d,\alpha)^{14}N$ nuclear reaction with the d^+ beam incident at 60° to the sample normal and the detector angle at 164°. The cross sections reported by Kim *et al.*[8] were used to calculate the oxygen concentration. The composition of the reaction product was determined using 2.0 MeV $^4He^+$ backscattering.

III. RESULTS AND DISCUSSION

In the course of our studies on the Ni/silicide and Si/silicide interfaces reported previously,[9] we observed that the intensity of the carbon and oxygen core level signals increased as the silicide reaction front advanced toward the sample surface. This was observed in Ni films deposited on amorphous Si (a-Si) as well as in a-Si films deposited on Ni. The oxygen impurity pileup at the interface resulted in a broad, low-intensity distribution on the high binding energy side of the Si 2p signal, corresponding to intermediate oxidation states of silicon. Previous investigators using Rutherford backscattering studies have reported that oxygen forms a diffusion barrier to the silicide reaction front and a number of suggestions have been made as to the nature of the barrier—e.g., Ni_2SiO_4, NiO, Ni_2O, SiO and SiO_2. The following experiments were therefore devised to examine the chemical details of the oxygen impurity derived barrier.

A. Controlled barrier formation

By monitoring the core level signals from the oxygen impurity as well as the silicon and nickel as a sample of Ni deposited on Si is heated *in situ*, one can follow the progression of the impurity atoms as the interfacial region advances into the observation depth of x-ray photoemission (~50 Å). Oxygen contamination is introduced into the Ni film in a controlled fashion using ion implantation. Three oxygen implant dosages were used, which correspond to peak intensities in the oxygen distribution of 1, 2, and 3 at.% of the Ni matrix. The *in situ* growth experiment is diagrammed in Fig. 1.

Figure 2 shows the progression of the O 1s intensity for each of these three dosages as a function of time during *in situ* silicide formation. Data for an unimplanted sample are also plotted. This as-deposited sample is representative of the

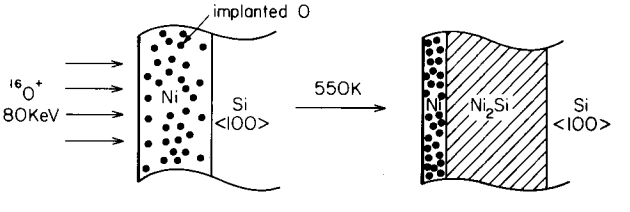

FIG. 1. Schematic representation of *in situ* silicide growth experiment.

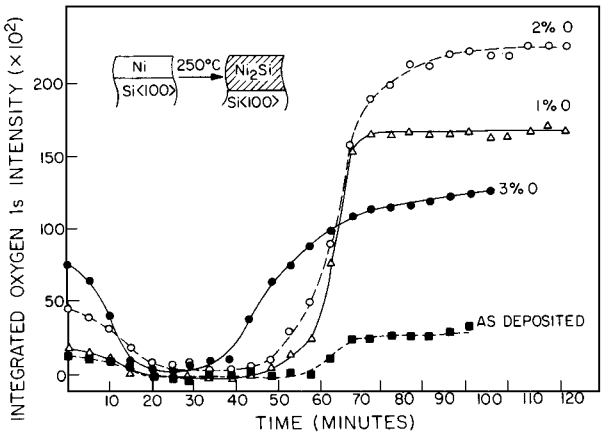

FIG. 2. Plot of the oxygen 1*s* spectral intensity as a function of time for various oxygen implant dosages.

amount of oxygen normally present in the Ni film as a result of oxygen contamination during the evaporation of the Ni film at 10^{-7} Torr. All four samples display an initial O 1*s* signal that decreases in intensity as the sample is heated. A finite amount of time is required for the sample to reach 550 K. The O 1*s* intensity has fallen to essentially zero in all cases after heating for 20 min, which corresponds to a sample temperature of ~480 K. We attribute this initial loss of oxygen signal to the desorption of oxygen containing contaminants present on the sample surface after the cleaning procedure. It is interesting that the amount of overlayer contamination increases with the implant dosage. This may be related to an increase in the surface damage or defects as the dosage increases. As time progresses and the Ni/Ni_2Si interface begins to advance toward the sample surface, the observed O 1*s* intensity increases rapidly. The onset of the increase in the impurity signal begins at ~35 min in the 3% implant. This is followed by the onset of the 2%, 1%, and as-deposited cases at 45, 50, and 60 min, respectively. The O 1*s* intensities eventually reach a maximum and remain constant throughout the remainder of the experiment. The maximum O 1*s* intensity obtained decreases in the order 2% > 1% > 3% > as-deposited. We attribute the apparent anomaly of the 3% O 1*s* maximum to the formation of a diffusion barrier as discussed previously.[3] In such a situation, the advance of the Ni/Ni_2Si interface is impeded by the formation of a barrier which prevents the diffusion of the Ni metal necessary to maintain the solid phase reaction. On the time-scale of the experiment, the Ni metal overlayer in the 3% case has not been consumed and it thus attenuates the signal from the oxygen that has accumulated at the Ni/Ni_2Si interface.

The final oxygen distributions for the samples used in the above experiments are shown in Fig. 3. These distributions were obtained using the $^{16}O(d,\alpha)^{14}N$ nuclear reaction. In this technique, a profile of oxygen is obtained from analysis of the energy distribution of α particles produced by the low energy bombardment of deuterons on the sample. The depth of the oxygen atoms is deduced from the fact that the observed energy of an α particle produced at some depth x depends on the energy loss suffered by the deuterons on reaching depth x and the energy loss of the subsequent α particle in traversing the sample before reaching the detector. The initial oxygen distribution before any reaction has occurred is shown by the dashed line in Fig. 3. After the samples were annealed *in situ* in the XPS spectrometer, the oxygen distributions indicated by the dotted curves were obtained. In each of the three cases, the oxygen had accumulated at or just below the sample surface. The concentration of oxygen calculated from these curves for the 1%, 2%, and 3% implant cases is 1.53×10^{16} cm^{-2}, 2.35×10^{16} cm^{-2}, and 2.96×10^{16} cm^{-2} ^{16}O, respectively. When compared to the original implant dosages, this corresponds to an increase in the oxygen concentration of 7.7×10^{15} cm^{-2}, 8.1×10^{15} cm^{-2}, and 6.2×10^{15} cm^{-2}, respectively. Because the samples were annealed in a background pressure of $\sim 2 \times 10^{-9}$ Torr, it is unlikely that the additional oxygen was introduced during the anneal step. We attribute the excess oxygen to oxidation of the sample surface that occurred during transport between the XPS apparatus and the nuclear-reaction measurements.

Once it has been established that the progression of the photoemission signals from the oxygen reflects the accumulation of oxygen at the Ni/Ni_2Si interface, the question of the chemical state of the oxygen can be addressed. Several possibilities exist: (1) the oxygen is bound in the Ni metal lattice in either substitutional or interstitial sites, (2) the oxygen is bound to the silicon atoms present at the Ni/Ni_2Si interface, or (3) the oxygen is present as a mixed compound such as nickel silicate, Ni_2SiO_4. To distinguish between these possibilities, the Ni and Si core-level signals were monitored as the Ni/Ni_2Si reaction front advanced into the observation depth of the spectroscopy. Figure 4 shows the final Si 2*p* spectra obtained as a function of the different ^{16}O implant dosages. In the 1%, 2%, and 3% oxygen-implanted samples, a large SiO_2 peak is observed on the high binding energy side of the Si 2*p* line from the Ni silicide. In the unimplanted sample, a broad peak of low intensity is present upfield of the substrate signal. Its position indicates the presence of Si^{+3} (Si_2O_3), Si^{+2}(SiO), and Si^{+1}(Si_2O) suboxides. The relatively weak intensity of Si 2*p* signal observed for the 3% implanted sample provides

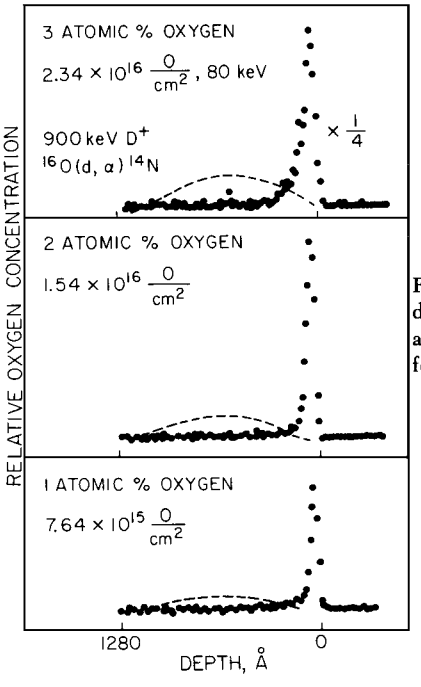

FIG. 3. Nuclear reaction depth profile of the oxygen after *in situ* silicide growth for various implant dosages.

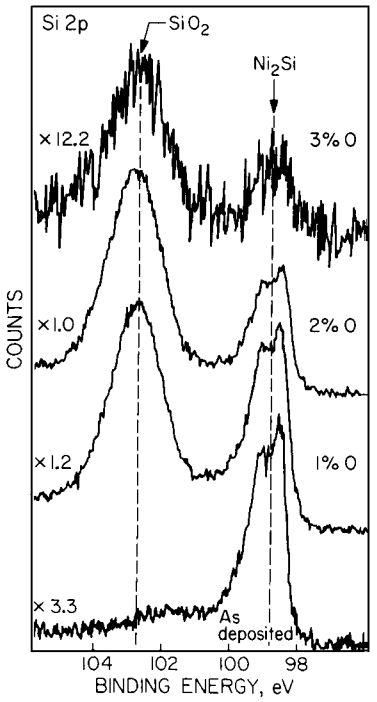

FIG. 4. Si 2*p* XPS spectra of the final silicide phase after *in situ* silicide growth for various oxygen implant dosages.

further evidence that the reaction front in this case has stopped before reaching the sample surface. The Ni/Ni_2Si interface must be within 50–100 Å of the surface in order for the Si 2*p* signal from the silicide to be detected by XPS. The ratio of the Si 2*p* oxide to Si 2*p* silicide integrated intensity is plotted in Fig. 5. There is a clear relationship between the amount of oxygen present in the Ni film before the reaction and the amount of SiO_2 observed after the reaction has been allowed to go to completion. Assuming the SiO_2 is present as a uniform layer above the silicide substrate, the ratio of the Si 2*p* oxide intensity, I_{ox}, to the Si 2*p* silicide intensity, I_{sil}, can be used to estimate the thickness x of the SiO_2 using the relationship

$$\frac{I_{ox}}{I_{sil}} = \frac{D_{ox}^{si}\lambda_{ox}}{D_{sil}^{si}\lambda_{sil}}\left(e^{x/(\lambda_{ox}\sin\theta)} + 1\right), \qquad (2)$$

where D_{ox}^{si} and D_{sil}^{si} are the atomic densities of Si in the oxide and silicide, respectively; λ_{ox} and λ_{sil} are the electron escape depths in the oxide and silicide, respectively; and θ is the angle between the plane of the sample and the detector. If we allow λ_{ox} to be 36 Å (Ref. 10) and assume a "metallic-like" escape depth of 15 Å for λ_{sil},[11] we calculate that the intensity ratios obtained for the unimplanted and the 1%, 2%, and 3% oxygen-implanted samples correspond to 3.5, 14.5, 17.4, and 24.0 Å, respectively. In the as-deposited and the 2% implant sample, analysis of the Ni 2*p* core level indicates the final reaction product is Ni_2Si. In the 1% implant case, the Ni 2*p* is somewhat higher in binding energy, indicating the reaction has been allowed to continue to the NiSi phase. In the 3% implant, only a Ni metal signal is observed. This is consistent with two features noted in previous figures: (1) the low intensity of the O 1*s* profile for the 3% implant in Fig. 2 indicates that the oxygen signal is attenuated by the presence of an overlayer, and (2) the relatively low intensity of the Si 2*p* signal for the 3% implant in Fig. 4 indicates that both the silicide and the silicon dioxide are attenuated by an overlayer. These observations indicate a barrier preventing the diffusion of Ni metal has been formed in the 3% implant sample. The Ni/Ni_2Si interface has stopped 50–100 Å from the sample surface. No such diffusion barrier is observed in the 1% or 2% implanted samples.

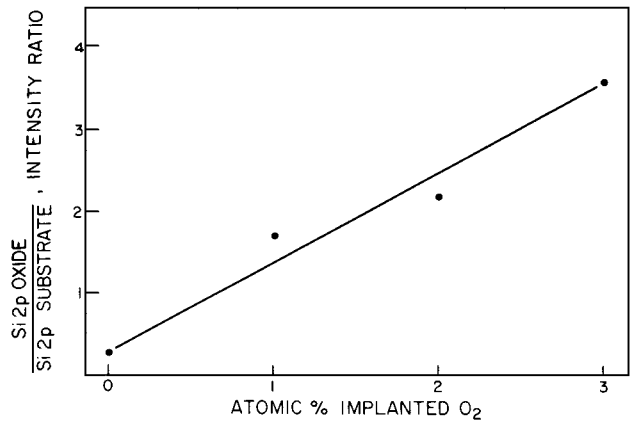

FIG. 5. Plot of the Si 2*p* oxide/substrate ratios for the spectra given in Fig. 4.

In the 3% implant sample, a total of 2.34×10^{16} $^{16}O^+/cm^2$ was implanted. The implanted oxygen has a gaussian profile with a peak maximum at 640 Å and a standard deviation of 330 Å. Assuming the Ni/Ni_2Si interface was stopped ~50 Å from the sample surface, as indicated by the XPS data, one can calculate the percent of the oxygen profile accumulated by the advancing interface. By integrating the gaussian distribution,[12] we determine that 94% of the implanted oxygen, or 2.2×10^{16} O/cm^2, has been accumulated. If the density of SiO_2 is taken to be 2.32×10^{22} molecules/cm^3, this thickness corresponds to ~ 45 Å. This estimate is higher than the 24 Å SiO_2 layer calculated above from the XPS data in Fig. 4. The difference in the estimates from the two techniques may be attributed to interfacial roughness. The XPS data should reflect a minimum value since the technique measures only an average SiO_2 layer thickness, as compared to the nuclear reactions which determine the actual atoms/cm^2.

To further elucidate the nature of the resulting thin films after reaction with 1%, 2%, and 3% implanted oxygen, $^4He^+$ backscattering was used. The backscattered spectrum corresponding to the 1% implant indicates that the thin-film reaction produced the first-phase Ni_2Si and then continued to consume entirely this phase to produce the second-phase NiSi. This agrees with the observed Ni 2*p* peak for the 1% implant, which indicates that NiSi is present on the sample surface. For the 2% case, the backscattered spectrum again indicates that the reaction has proceeded to the second-phase NiSi. However, there is the additional presence of a small surface peak in the backscattered spectrum. This peak is resolution-limited and, since backscattering is a bulk technique, one is unable to determine the Ni to Si ratio in this surface region. The XPS Ni 2*p* spectrum obtained for the 2% implant, however, indicates that the sample surface consists of the first-phase compound Ni_2Si. This suggests that the oxygen that had accumulated at the Ni/Ni_2Si interface was insufficient to block the complete formation of the Ni_2Si, but

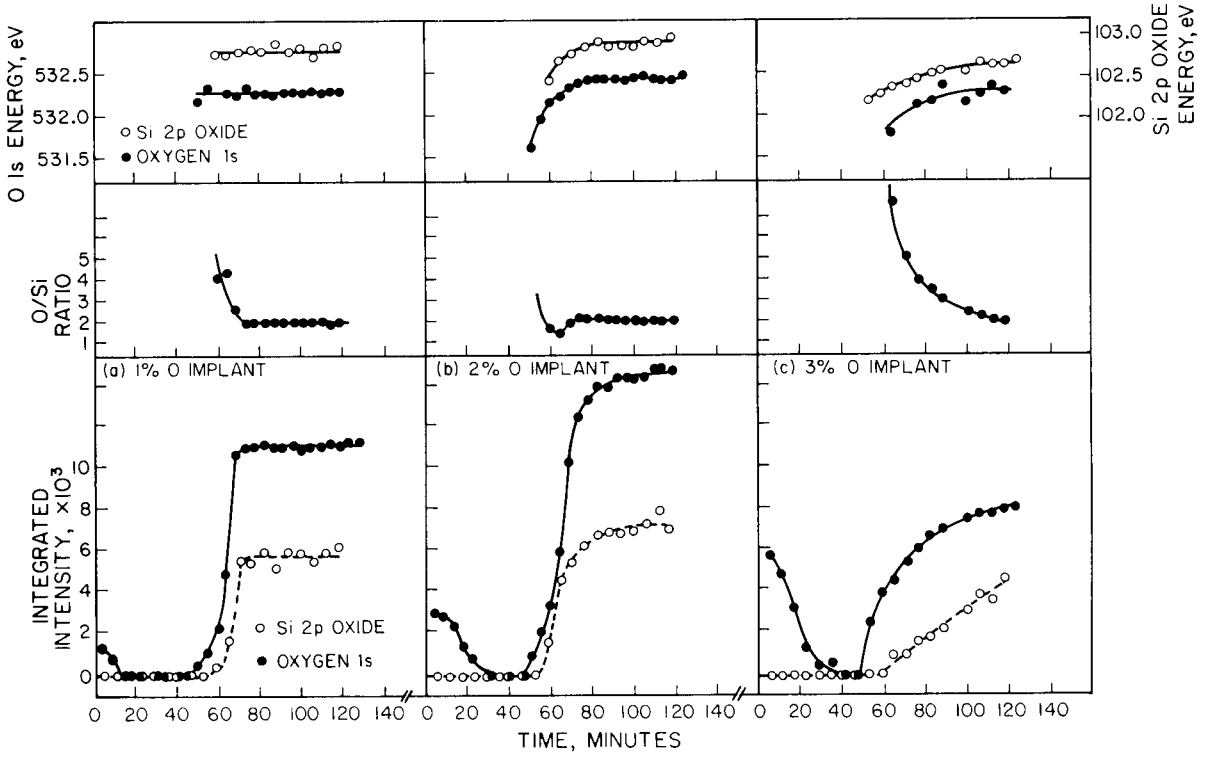

FIG. 6. Plot of the Si 2*p* and O 1*s* core line intensities, O/Si stoichiometries, and binding energy maxima as a function of time for (a) 1% oxygen, (b) 2% oxygen, and (c) 3% oxygen implant dosages.

that it was suffient to prevent the NiSi reaction from completely consuming the Ni_2Si. This is the first evidence for the blockage of the second-phase silicide formation by an impurity barrier. Finally, in the 3% implanted sample, a backscattered spectrum identical to that found for the 2% case is obtained. The XPS spectra indicate that in this case, however, the species present on the sample surface is Ni metal. The oxygen impurity level was sufficiently high that it blocked the diffusion of the Ni metal and thus prevented the Ni/Ni_2Si interface from reaching any closer than 50–100 Å of the sample surface. Once the Ni diffusion was blocked, the second-phase NiSi began to form at the Si/Ni_2Si interface. This phase proceeded to consume the Ni_2Si until it too was within 50–100 Å of the sample surface.

The XPS data has thus far suggested that the formation of SiO_2 is responsible for the barrier against Ni metal diffusion. The possibility that Ni oxide is participating in the barrier can be excluded by examining the Ni 2*p* core levels. The compound NiO falls at a binding energy of 854.0 eV. No structure is observed in Ni at this energy in the final Ni 2*p* spectra, nor is any evidence found for the existence of Ni_2SiO_4 or like compounds.

If all the oxygen present in the film is bound as SiO_2, then the O 1*s* intensity should be completely accounted for by the Si 2*p* oxide intensity. In the lower panel of Fig. 6(a), the Si 2*p* oxide and O 1*s* intensities are plotted as a function of time as the Ni/Ni_2Si interface advances toward the sample surface. The initial decrease in the O 1*s* signal is due to the desorption of oxygen containing impurities on the sample surface as the temperature increases. During the first 45 min of the *in situ* reaction, no O or Si signal is detected. After 45 min, the O 1*s* signal begins to increase rapidly followed by the Si 2*p* oxide signal after 53 min. After 70 min, both signals have attained their maximum intensity and remain constant for the remainder of the experiment. The observation that the O 1*s* signal begins to increase before the Si 2*p* oxide is significant. It cannot be accounted for by a difference in electron escape depths. The kinetic energy of the Si 2*p* photoelectron is greater than that of the O 1*s* photoelectron. On this basis alone, one would expect to observe the Si 2*p* signal before the O 1*s*. That the opposite occurs suggests that there must be a front of oxygen preceding the SiO_2 layer. This is also indicated by the O/Si stoichiometry ratio plotted in the middle curve of Fig. 6(a). A O/Si ratio of 2 indicates stoichiometric SiO_2. The experimentally measured (O 1*s*)/(Si 2*p*) intensity ratios were calibrated against a thick thermal SiO_2 oxide on Si. The use of a calibration standard allows the estimation of the stoichiometry because such unknown factors as the photoelectron cross sections and electron escape depths are intrinsically included. In Fig. 6(a), it can be seen that the initial onset of O 1*s* intensity corresponds to an O/Si ratio considerably greater than 2. This indicates that initially more oxygen is present than can be accounted for by SiO_2. When the O 1*s* and Si 2*p* signals have attained their maximum intensity, the O/Si ratio is 2. At the end of the reaction, all oxygen can be accounted for by the formation of SiO_2. No additional oxygen is present in other chemical species. The upper curves in Fig. 6(a) plot the O 1*s* and Si 2*p* oxide binding energies as the interface advances. Both the O and Si signals remain constant at 532.3 and 102.9 eV, respectively.

The O 1*s* and Si 2*p* oxide intensities for the 2% implanted sample are plotted as a function of time in the lower curve of Fig. 6(a). Qualitatively, the curves are similar to those obtained with the 1% sample. The O 1*s* signal is observable after

~45 min, while the Si 2*p* oxide line first appears after ~55 min. This suggests that there is an oxygen front prior to the SiO_2 as in the 1% implant. The O/Si ratio is greater than 2 in this region. After ~90 min, the O and Si intensities reach a plateau. At this point, the O/Si ratio is 2, indicating the presence of SiO_2 with no excess oxygen. The dip in the O/Si curve indicates the presence of silicon suboxides in front of the SiO_2 region. The O 1*s* and Si 2*p* oxide binding energies in the upper curves show a gradual shift from low to high binding energies as the initial signals appear. This further indicates that at least some of the excess oxygen in this region is bound as a Si suboxide such as those noted previously in the as-deposited sample. The striking difference between the 2% and 1% sample is that the increase of the Si 2*p* oxide and O 1*s* intensities to their plateau is considerably more gradual in the 2% implant. This indicates that although no barrier to Ni diffusion has formed, the reaction rate has decreased. This is consistent with work reported by others on the effect of oxygen impurities on the growth kinetics of silicides.[1–3]

The decrease in the growth rate of nickel silicide is more dramatic in the 3% implanted samples as shown in the lower curve of Fig. 6(c). In this case, 120 min are required for the O and Si signals to begin to reach their maximum intensities. As in the 1% and 2% samples, the early onset of the O 1*s* intensity and the large O/Si ratio indicates a front of oxygen must precede the SiO_2 layer. The gradual upfield shift of the Si 2*p* oxide binding energy suggests the presence of Si suboxides preceding the stoichiometric SiO_2.

B. Chemical bonding in the Si/O system

In our previous work,[4] we have discussed the use of the XPS-derived chemical shift as a measure of bonding and valence charge redistribution. There we pointed out that the XPS binding energy was determined by two terms: (1) the number of Si–O–Si or Si–O bonds formed about the silicon tetrahedron, and (2) the detail of the bridging angle of the Si–O–Si bond. This latter term is derived from the strong change in valence charge distribution as a function of orbital overlap. This effect was modeled by a tight-binding calculation and empirically correlated with the observed chemical shift for a variety of Si,O compounds. In this analysis (SICT), we suggested that strain arising from lattice mismatch would cause a change in bond-angle distribution and, correspondingly, a change in Si–O charge transfer. Unfortunately, as noted in Eq. (1) of the introduction, XPS binding energies are generally regarded as comprising a chemical shift and a relaxation term. The extra atomic component of the relaxation energy generally dominates when comparing the same core levels and relatively similar chemistry. This relaxation contribution is generally believed to follow the density of states at the Fermi level. Consequently, this term is largest for metals and semi-metals, smaller for semiconductors, and smallest for insulators.

We have demonstrated in the preceding that we have fabricated in this experiment thin films, 5–25 Å thick, comprising SiO_2, Si_2O_3, SiO, and Si_2O. Further, these films are sandwiched between a metal overlayer and a metallic or semimetal substrate. Because of the film thickness and its proximity to the metallic overlayers, the relaxation effects for these different species should be nearly identical. Consequently, comparison of relative chemical shifts between compounds in this environment should give a measure of the true chemical shift. The significant difference in lattice parameters between Si^0 and Ni_2Si substrates should lead to a change in bond angle and, correspondingly, a test of the SICT model.

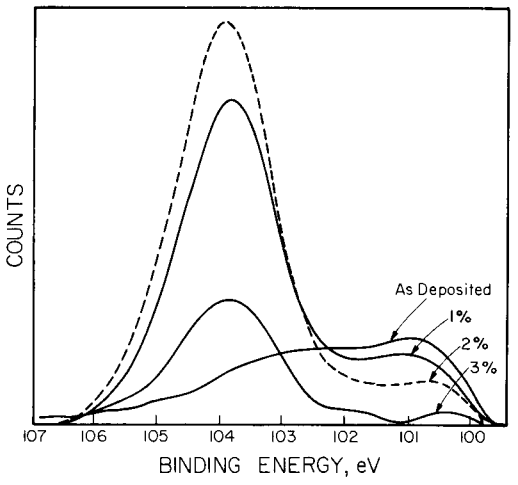

FIG. 7. Difference curves for the Si 2*p* spectra shown in Fig. 4. The silicide substrate lineshape has been subtracted.

In Fig. 7, we give the spectra of Fig. 4 after subtraction of the Ni_2Si substrate and after smoothing with a Weiner filter.[13] In these we see that increasing the concentration of oxygen in the starting metal host leads to a reduction in the amount of Si^{+1}, Si^{+2}, and Si^{+3} species in favor of increased SiO_2 intensity. The as-deposited case has the lowest oxygen content and, correspondingly, the largest amount of reduced oxide. The 3% implant case seems to show only Si^{+4} and Si^{+3} states.

In previous work, we have suggested that the binding energy difference between two core levels corresponding to adjacently bonded atoms is the best measure of valence electron redistribution or charge transfer, and, therefore, different bonding detail. Those binding-energy differences between the Si 2*p* and the O 1*s* lines are tabulated in Table I. This computation includes the results of this work (referenced to the position of Ni_2Si) along with a number of previous investigations.

Note that the binding energies cited for the 3% oxygen implant show a significantly smaller charge transfer Si → O as compared to the 1% and 2% cases. The O 1*s*–Si 2*p* energy difference for SiO_2 on the top of Ni_2Si is only 0.1 eV different than that observed for SiO_2 on Si^0. With the intact Ni overlayer, however, this number becomes 430.2 eV which is 0.6 eV larger than that obtained for the a-SiO_2. We therefore suggest that the shift in these numbers is consistent with strain-induced charge-transfer (SICT) arguments. This investigation will continue with the use of other metals as impurity hosts thereby growing these oxides on different substrates and with different effective encapsulants. The results will be the subject of future publications.

The chemical shift for SiO_2 relative to elemental Si for the 3% case is 3.68 eV. This case corresponds to a double sandwich structure and is therefore most likely to be a relaxation-free

TABLE I. Tabulation of Si 2*p* (oxide—element) and O 1*s*–Si 2*p* (oxide) binding energy differences.

Compound	ΔSi2*p* (oxide—element)	O1*s*-Si2*p* (oxide)	References
a-SiO_2	4.1 eV	429.6 eV	18, 16
α-quartz	...	429.7	19
CVD-SiO_2	4.1	429.6	20
120°-SiO_2	4.0	430.6	17, 18, 4, 16
144°-SiO_2	4.5	429.5	17, 18, 4, 16
(168–180°)-SiO_2	5.4	427.9	17, 18, 4, 16
Si_2O_3	2.9	432.6	17, 18, 16
Si_2O_3 (siloxene)	3.4	430.0	6
SiO (Si/SiO_2)	1.7	432.6	17, 18, 16
SiO	2.2	431.0	21
SiO (siloxene)	2.1	431.4	6
Si_2O (Si/SiO_2)	0.6	432.8	17, 18, 16
Si_2O	0.8	432.4	17, 18, 16
Si_2O (siloxene)	0.5–0.8	432.8	6
SiO_2 (Ni_2Si/Ni)			
1% O (14 Å)	4.3	429.3	This work
2% O (18 Å)	4.3	429.4	This work
3% O (24 Å)	3.68	430.2	This work
as-dep (4 Å)			
SiO_2 (Ni_2Si/Ni)	4.4	...	This work
Si_2O_3 (Ni_2Si/Ni)	3.3	...	This work
SiO (Ni_2Si/Ni)	2.1	...	This work
Si_2O (Ni_2Si/Ni)	0.9	...	This work

comparison. In a recent discussion of relaxation effects for Si^0, Si^{+1}, Si^{+2}, Si^{+3}, and Si^{+4} for the Si 2*p* lines, Bechstedt[14] derived a value of 0.87 eV as the relaxation difference between Si^0 and Si^{+4}. If we subtract this value from the normally observed value of 4.5 eV binding-energy difference between element and SiO_2, the true difference in chemical shift would be 3.63 eV—in surprising agreement with the value of 3.68 derived in this experiment.

Addressing the general question of the existence of the intermediate oxides of silicon, we have plotted an expansion of the Si 2*p* spectrum of the as-deposited case in Fig. 8. Together with the raw data, we plot the resolution-enhanced reconstruction of the spectrum which gives four basic oxide peaks plus the substrate peak within the spectral envelope. This analysis has been described previously,[4,15,16] and is particularly sensitive to the presence of peaks in a spectrum. The separation of these peaks corresponds to low-frequency information in the Fourier transform and is therefore consistent with the observed signal/noise ratio. The reconvolved curve (including the Si 2*p* spin orbit doublet) is also plotted in the curve and is seen to pass smoothly through the noise packet of the raw data. The separation between these peaks is reported in Table I, as are the Fermi-level referenced binding energies. These numbers show substantial agreement with those reported at the Si/SiO_2 interface,[4] and in our synthetic and radiation-damage efforts.[6,7]

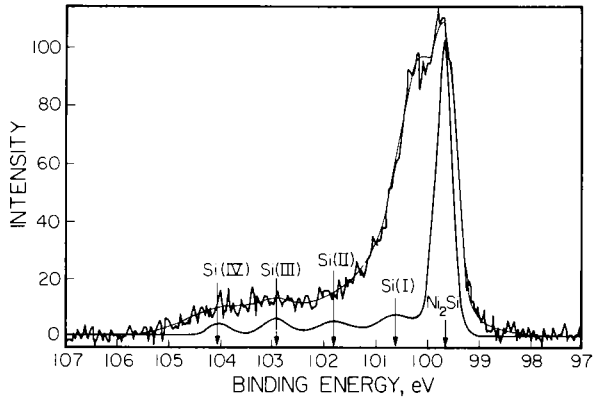

FIG. 8. Plot of the as-deposited Si 2*p* line with a resolution-spectrum and its reconstruction.

IV. CONCLUSIONS

In this paper, we have examined the effect of implanted oxygen on the Ni/Ni_2Si interface using XPS, $^4He^+$ backscattering, and $^{16}O(d,\alpha)\,^{14}N$ nuclear reactions. Analysis of the Ni, Si, and O core levels demonstrates that the formation of SiO_2 is responsible for the Ni diffusion barrier rather than Ni oxide or mixed oxides such as Ni_2SiO_4. It was determined that 2.2×10^{16} O/cm^2 is sufficient to prevent Ni diffusion under UHV annealing conditions.

At low oxygen impurity levels, Si suboxides (Si_2O_3, Si_2O, SiO) are formed as the advancing interface encounters oxygen in the Ni matrix. This provides a novel approach for synthesizing these suboxides, which are not normally found as bulk compounds, to provide model structures for Si/SiO_2 interfacial studies. Because these Si oxides and suboxides are sandwiched between metallic matrices, relaxation effects in XPS can also be examined. We find the chemical shift of SiO_2 relative to Si^0 in such a metal sandwich is 3.68 eV, which agrees well with the normally observed chemical shift corrected for the difference in relaxation between Si^0 and SiO_2. Finally, the change in the observed O 1*s*–Si 2*p* (oxide) binding energy difference from 429.4 to 430.1 eV for thermal SiO_2 as compared to SiO_2 in the metal matrix is consistent with structure-induced charge transfer arguments discussed in previous work.[4]

[a]This work presents the results of one phase of research performed at the Jet Propulsion Laboratory, California Institute of Technology, sponsored by the National Aeroonautics and Space Administration under Contact NAS7-100 and the Office of Naval Research (L. R. Cooper).

[1]C. A. Crider and J. M. Poate, Appl. Phys. Lett. **36**, 417 (1980).
[2]J. B. Bindell, J. W. Colby, D. R. Wonsidler, J. M. Poate, D. K. Conley, and T. C. Tisone, Thin Solid Films **37**, 441 (1976).
[3]D. M. Scott, P. J. Grunthaner, B. Y. Tsaur, M-A. Nicolet, and J. W. Mayer, in the *Proceedings of the Symposium on Thin-Film Interfaces and Interactions* (Electrochemical Society, Princeton, N.J., 1980).
[4]F. J. Grunthaner, P. J. Grunthaner, R. P. Vasquez, B. F. Lewis, J. Maserjian, and A. Madhukar, Phys. Rev. Lett. **43**, 1683 (1979).
[5]F. J. Grunthaner, B. F. Lewis, R. P. Vasquez, J. Maserjian, and A. Madhukar, *The Physics of MOS Insulators*, edited by G. Lucovsky, S. T. Pantelides, and F. L. Galeener (Pergamon, New York, 1980), Chap. VII, p. 290.
[6]J. A. Wurzbach, *The Physics of MOS Insulators*, edited by G. Lucovsky, S. T. Pantelides, F. L. Galeener (Pergamon, New York 1980), Chap. IV, p. 172.
[7]F. J. Grunthaner, B. F. Lewis, N. Zamani, J. Maserjian, and A. Madhukar, IEEE Trans. Nucl. Sci. **NS-27**, 1640 (1980).
[8]H. C. Kim, R. F. Seiler, D. F. Herring, and K. W. Jones, Nucl. Phys. **57**, 526 (1964).
[9]P. J. Grunthaner, F. J. Grunthaner, and J. W. Mayer, J. Vac. Sci. Technol. **17**, 924 (1980).
[10]J. M. Hill, D. G. Royce, C. S. Fadley, L. F. Wagner, and F. J. Grunthaner, Chem. Phys. Lett. **44**, 225 (1976).

[11]D. R. Penn, J. Electron Spectrosc. Relat. Phenom. **9,** 29 (1976).
[12]P. R. Bevington, *Data Reduction and Error Analysis for the Physical Sciences* (McGraw-Hill, New York, 1969).
[13]K. R. Castleman, *Digital Image Processing* (Prentice-Hall, Englewood Cliffs, New Jersey, 1979).
[14]F. Bechstedt, Phys. Status Solidi (b) **91,** (1979).
[15]R. P. Vasquez, J. D. Klein, J. J. Barton, and F. J. Grunthaner, J. Electron Spectrosc. Relat. Phenom. **23,** 63 (1981).
[16]F. J. Grunthaner, P. J. Grunthaner, R. P. Vasquez, B. F. Lewis, J. Maserjian, and A. Madhukar, J. Vac. Sci. Technol. **16,** 1443 (1979).
[17]F. J. Grunthaner and J. Maserjian, IEEE Trans. Nucl. Sci. **NS-24,** 2108 (1977).
[18]F. J. Grunthaner and J. Maserjian, in *The Physics of SiO_2 and its Interfaces*, edited by S. T. Pantelides *et al.* (Pergamon, New York, 1980), p. 389.
[19]D. A. Stephenson and N. J. Binkowski, J. Non-Cryst. Solids **22,** 399 (1976).
[20]R. P. Vasquez and F. J. Grunthaner, Surf. Sci. **99** (3), 681 (1980).
[21]S. I. Raider and R. Flitsch, J. Electrochem. Soc. **123** (11), 1754 (1976).